remote sensing

MDPI

Article

Crop Mapping Using Sentinel-1 and Sentinel-2 Imagery and UAV-Acquired Ground-Truth Data: Pilot Study in Rwanda

Meghan Hegarty-Craver [1,*], Jason Polly [1], Margret O'Neil [1], Noel Ujeneza [2], James Rineer [1], Robert Beach [1], Daniel Lapidus [1], and Dorota S. Temple [1]

[1] RTI International, Research Triangle Park, NC, USA; 27709; mhegarty@rti.org; jpolly@fclwd.com; maggieo@rti.org; jrin@rti.org; rbeach@rti.org; dlapidus@rti.org; temple@rti.org
[2] Independent agri-consultant, Kigali, Rwanda; nujeneza@gmail.com
* Correspondence: mhegarty@rti.org

Received: date; Accepted: date; Published: date

Abstract: Timely and accurate agricultural information is needed to inform resource allocation and sustainable farming practices leading to improved food security for the developing world. Remote sensing technologies can be leveraged to provide cost-effective data. Machine-learning models have been used to create cropped land area maps using freely available satellite data, but these models are heavily dependent on the quality of the training data. For example, in applications focused on identifying areas of individual crop types, ground-truth locations must be georeferenced accurately and labeled correctly. Achieving this accuracy is difficult in smallholder agricultural systems, especially when fields are intercropped. In this pilot study, we used imagery acquired from unmanned aerial vehicles to create a high-fidelity ground-truth dataset that was used to train and test a random forest model for classifying cropped land using freely available Sentinel-1 and -2 data. This model achieved an overall accuracy of 83%, and a 91% accuracy for maize specifically. The model results were also compared with the seasonal agricultural survey which highlighted biases in the dataset including a lack of examples of cells with mixed land cover.

Keywords: Sentinel-1, Sentinel-2, Google Earth Engine, unmanned aerial vehicles, smallholder agriculture, machine-learning models

1. Introduction

The potential of satellite-based remote sensing to provide information on agricultural production has been recognized since the mid-1970s [1,2]. Thanks to the launch of the Sentinel satellites, images of the Earth with ground resolution of 10 m have recently become freely available [3]. This development opened the door to monitoring agricultural activity in smallholder farming systems [4-7]. In a parallel development, open-access cloud-based computing infrastructure [8,9] has made it practical and cost-effective to process high-resolution images and extract information relevant to crop mapping. Recognizing this change of paradigm, the Food and Agriculture Organization (FAO) of the United Nations in its "Global Strategy to Improve Agricultural and Rural Statistics, Phase 2, 2020-2025" identified remote sensing as an important component of its research agenda, calling for new data and methodologies to enable high-accuracy, high-refresh crop mapping and crop yield estimation [10-12].

Crop maps are typically generated using supervised machine-learning (ML) models [11,13]. To train a model, a human analyst uses ground observations to identify locations of a specific crop and then extracts signal values from satellite images acquired for these locations. The ML algorithm uses the training data to learn spectral signatures of the crops. The trained model is then applied to a large-

area satellite image of interest, and the algorithm assigns each pixel of the image to the crop class that best matches the learned signatures. The result is a crop map from which areas under cultivation can be calculated for each crop [14,15].

A key aspect in developing well-performing ML models is the quality of ground-truth data [11]. The ground-truth locations must be accurately georeferenced and reliably labeled with the correct crop type. For this reason, some studies [16] rely on training data that have been collected from sites that are managed by the Joint Experiment for Crop Assessment and Monitoring [17]. These sites are rigorously monitored for the purposes of generating time-series datasets and improving agricultural models using remote sensing data; however, the number of these sites is limited. Others rely on continental- or regional-scale cropland data maps for generating ground truth [18,19], but these types of maps cannot be rendered with a high degree of accuracy for the developing world because of sparse and/or missing data [20]. For smallholder agricultural systems, information is traditionally obtained by observers on the ground [6,20-22]. Aside from practical limitations such as the challenge of surveying hilly or remote areas with limited road systems, this practice is time consuming, is labor intensive, and does not lend itself to easy standardization and automation.

In recent years, unmanned aerial vehicles (UAVs) have become widely available and inexpensive, and companies providing UAV services are now present in many developing countries. UAVs can acquire high-resolution georeferenced images of large areas quickly and at low cost [23,24]. For example, in this study, images of an area of 80 ha with a ground resolution of 10 cm were obtained in 2 to 3 hours. UAV imagery can be georeferenced with high accuracy, reliably registering locations of even the smallest fields in the satellite grid. The aerial view gives the analyst the ability to accurately label intercropped fields, a task that is especially difficult for surveyors on the ground [25]. Although UAV-acquired images have previously been employed to gain information about agricultural production on a local scale [26-31], their use as a source of ground-truth data for satellite-based crop analytics has not yet been widely investigated [32].

The objective of this study was to pilot a UAV-based ground-truth data acquisition methodology to enable the development of crop-mapping models applicable to freely available Sentinel-1 and Sentinel-2 imagery. Rwanda, a small country in sub-Saharan Africa, was selected for this pilot study. Although the Rwandan government conducts seasonal agricultural surveys, it also recognizes the potential of satellite-based crop analytics to provide additional and timely (e.g., during the growing season) information to support planning for food security and sustainability [33-35]. Smallholder agriculture dominates the country; therefore, existing low-resolution continental-scale cropland maps are of limited value for either monitoring agricultural activity or training ML models. The UAV images we obtained during this study were labeled as to the type of land cover/crop by human analysts. We then extracted Sentinel-2 MSI (multispectral instrument) and Sentinel-1 SAR (synthetic aperture radar) signal values from images obtained on selected dates for the labeled locations to create the training dataset for the ML model. Given the significant cloud cover during the 2019 Season A (September 2018–February 2019), we chose to focus the training, testing, and implementation of the ML model on relatively cloud-free Sentinel-2 (S2) images recorded in January 2019, when, serendipitously, many crops reached their maturity and tended to exhibit the most pronounced differences in their spectral signatures [36]. We tested the ML model on a subset of the ground-truth dataset that was not used for training. The model was applied to two cloud-free January images to create a composite map of Rwanda showing areas planted with specific crops at a 10-m scale. To further assess the model, we compared the areas under specific crops with the areas reported by the agricultural survey for 2019 Season A, obtaining agreement for maize and beans to within 10% at the country scale.

2. Materials and Methods

2.1. Study Site

This pilot study was conducted in Rwanda (Figure 1), a small country (approximately 25,300 km^2 [36]) located in sub-Saharan Africa. Agriculture represents 24% of Rwanda's gross domestic

product [37]. Fields in Rwanda are small (often <1 ha) and intercropped, although larger mono-cropped fields (consolidated land use areas) do exist. The crop calendar reflects two main seasons: Season A extends from September through February, and Season B extends from March through June [36]. The starts and ends of the agricultural seasons, however, depend on the type of crop being grown, the region of the country, and the onset of rain. The major crops grown in Rwanda are maize, beans, bananas, and roots and tubers such as cassava, potatoes, and sweet potatoes.

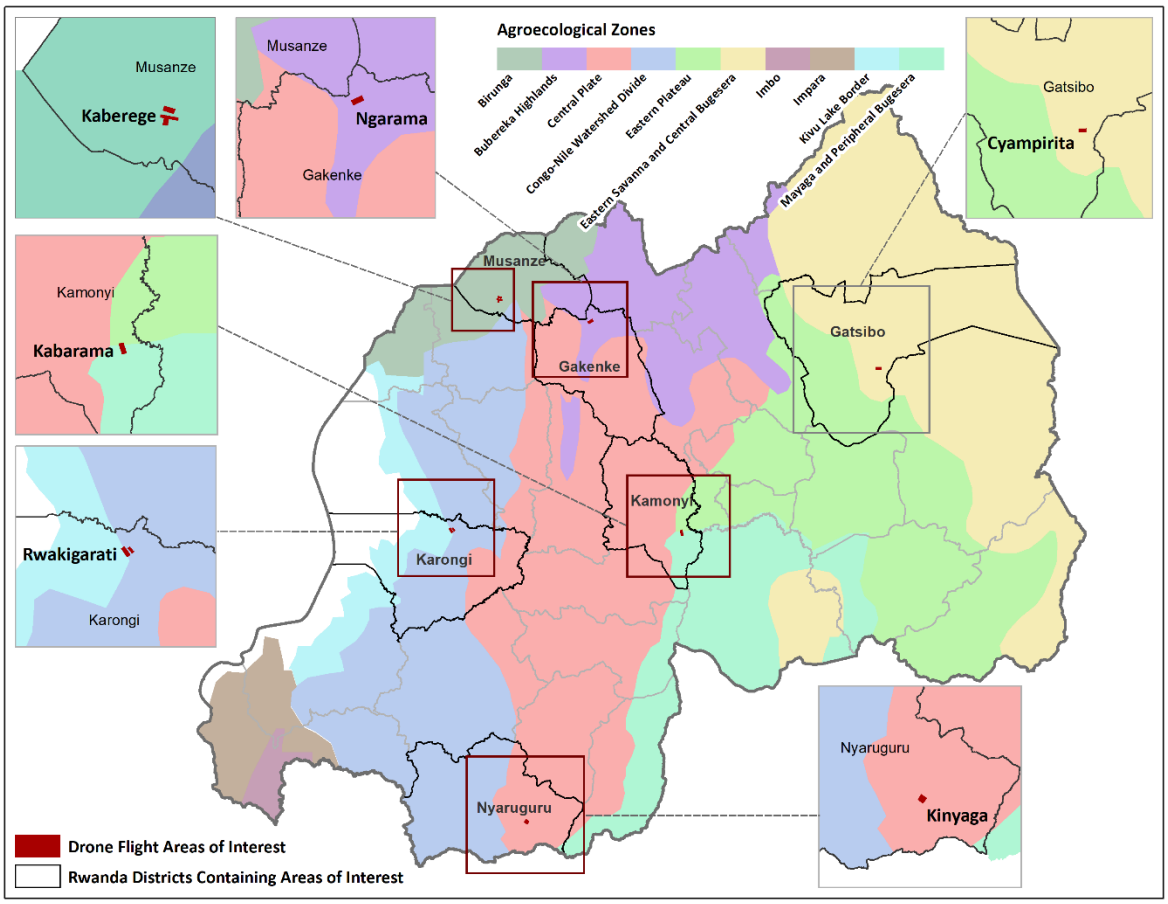

Figure 1. Agro-ecological zone map of Rwanda with UAV flight sites and districts noted

Source: Chew, Rineer, Beach, O'Neil, Ujeneza, Lapidus, Miano, Hegarty-Craver, Polly, and Temple [38].

2.2. Ground-Truth Data

For the ground-truth dataset, we collected high-resolution imagery in a series of UAV flights that were conducted at six locations in different agro-ecological zones (AEZs) [39,40] (Figure 1). AEZs in Rwanda are mainly divided along the lines of elevation (higher elevation in the west and north and lower elevation toward the east), rainfall (higher in the west and lower in the east), and temperature (higher in the east and lower in the west) [40]. Sites within these AEZs were selected based on accessibility and the presence of (1) consolidated land use areas where field sizes are larger and generally only a single crop is grown; (2) smaller, intercropped fields that represent the dominant practice of smallholder agriculture; and (3) natural areas. Flights covered approximately 80 ha in each location and were conducted on three dates during the peak of the 2019 Season A growing season. This information is summarized in Table 1.

The UAV flights were conducted by Charis Unmanned Aerial Solutions (Kigali, Rwanda). Camera and UAV selections were based on the site requirements on the day of the flight. The UAVs used in this study were the DJI Inspire (DJI, Shenzhen, China), Ebee plus (senseFly SA, Cheseaux-sur-Lausanne, Switzerland), and the Parrot Disco (Parrot, Paris, France). The RGB (red, green, blue) cameras used in this study were the SONY ILCE-6000 (SONY, New York, NY, USA), DJI Zenmuse

X5S (DJI, Shenzhen, China), and senseFly S.O.D.A. (senseFly SA, Cheseaux-sur-Lausanne, Switzerland).

Table 1. UAV flight site information.

Location	Agro-Ecological Zone	Flight #1	Flight #2	Flight #3
Kaberege	Birunga	Dec. 27, 2018	Jan. 29, 2019	Feb. 19, 2019
Kinyaga	Central Plate/Eastern Plateau	Dec. 12, 2018	Jan. 24, 2019	Feb. 21, 2019
Kabarama	Mayaga and Peripheral Bugesera	Dec. 10, 2018	Jan. 21, 2019	Feb. 16, 2019
Cyampirita	Eastern Savanna and Central Bugesera	Dec. 17, 2018	Jan. 25, 2019	Feb. 18, 2019
Ngarama	Buberuka Highlands	--	Jan. 30, 2019	Feb. 20, 2019
Rwakigarati	Congo-Nile Watershed Divide/Kivu Lake Border	Dec. 27, 2018	Jan. 31, 2019	Feb. 22, 2019

For labeling, the orthomosaic RGB images from each flight (nominal resolution of 3 to 10 cm) were imported into a custom viewer that used ESRI's ArcGIS API for JavaScript and ArcGIS Enterprise (ESRI, Redlands, CA, USA). The viewer was designed to support multiple users simultaneously, tracking user and date of entry. The 10-m x 10-m Sentinel pixel grid was overlaid on the UAV images in the viewer. To avoid labeling locations corresponding to S2 pixels covered by clouds in the images of interest, we created a shapefile representing these clouded pixels and applied it to mask the clouded locations in the viewer. Grid cells were labeled according to the dominant landcover (i.e., at least 75% of the cell was the same class), and cells were not labeled in clouded areas. For this pilot study, we limited the number of classes to four strategic crops, a "catch-all" class for other crops and grasslands, a class for trees and woodlands, and a catch-all class for non-vegetative land covers. The classes are as follows:

1. Maize
2. Beans (bush beans and climbing beans)
3. Cassava
4. Bananas (all varieties)
5. Other vegetation (OtherVeg) representing grassland and crops not in class 1 through 4
6. Trees representing small tree stands, forest, and woodlands
7. Non-vegetative (NonVeg) land cover representing bare ground, buildings, structures, and roads

Figure 2 shows examples of labeled sections of UAV images for each of the selected classes. Each example corresponds to an area of 10-m x 10-m on the ground. The number of ground-truth examples for each of the six UAV flight sites is detailed in Table 2. Emphasis was placed on labeling points from the Kaberege, Kinyaga, Kabarama, and Cyampirita sites for which cloud-free satellite images were available during the peak of the growing season; the Ngarama and Rwakigarati sites were heavily clouded then. Within the cloud-free sites, we tried to balance the number of labeled examples. In total, we created 1,251 labeled data points. At least 100 points were targeted for each class and, ideally per AEZ, as a typical rule of thumb for the minimum size. These data points were originally labeled by researchers who were trained by Mr. Noel Ujeneza who is a Rwandan agricultural expert and a co-author of this study. Mr. Ujeneza also accompanied the UAV operators to the test sites on several occasions and reviewed the labeled cells for accuracy. Furthermore, we cross-referenced the labeled cells between the December and January flight dates to ensure that the ground cover designation was consistent (note: in the February flights, it was apparent that harvest had already occurred in many areas, and we did not rely on these data for labeling). Cells not meeting this criterion were eliminated. Cells were also denoted as good, average, or poor examples of ground cover as related to the health of the vegetation, and cells labeled as poor were eliminated.

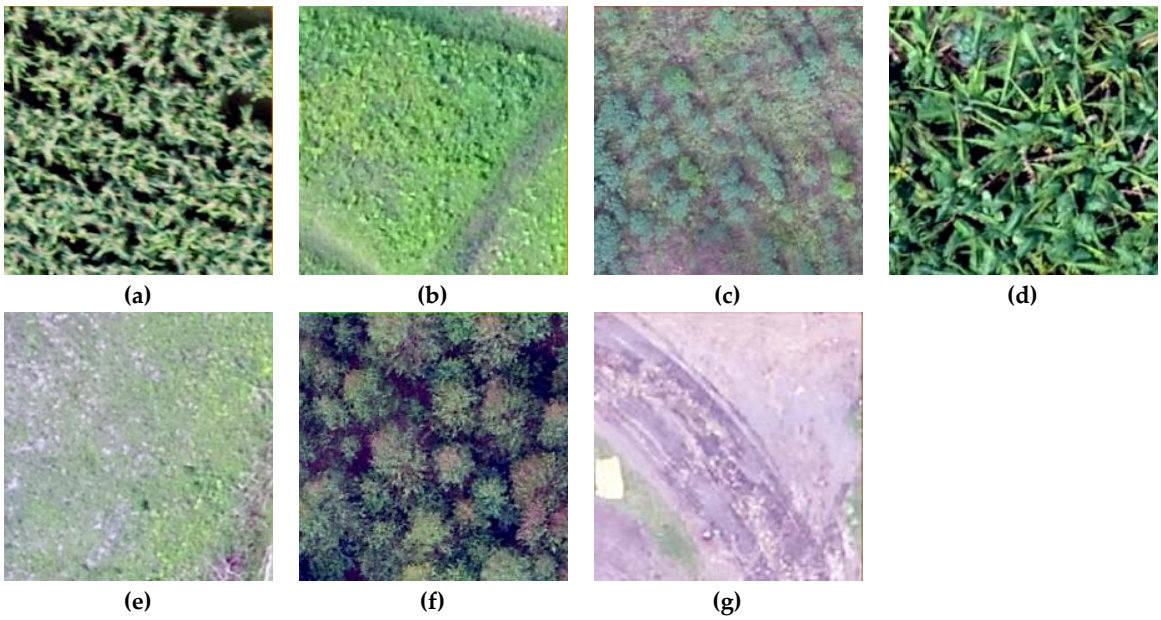

Figure 2. Examples of 10-m x 10-m sections of UAV images representing selected categories: (a) Maize, (b) Beans, (c) Cassava, (d) Bananas, (e) OtherVeg, (f) Trees, (g) NonVeg.

Table 2. The number of ground-truth data points by class by site (Kbg = Kaberege, Kin = Kinyaga, Kbm = Kabarama, Cym = Cyampirita, Nga = Ngarama, Rwa = Rwakigarati).

Class	Kbg	Kin	Kbm	Cym	Nga	Rwa	Total
Maize	130	37	11	101	8	2	289
Beans	33	8	69	20	7	7	144
Cassava	0	17	53	47	6	12	135
Bananas	4	12	42	14	9	4	85
OtherVeg	12	46	29	47	0	9	143
Trees	105	30	56	104	0	0	295
NonVeg	37	38	29	26	5	25	160
Total	321	188	289	359	35	59	1,251

2.3. Satellite Data Processing

We used optical images from the S2 satellite and SAR images from the S1 satellite. S2 optical images represent reflectance of light from the Earth's surface as a function of the wavelength of the light. For crops, this spectral reflectance is determined by the plant's biophysical and biochemical properties, such as the leaf area, biomass, chlorophyll content, water content, and canopy structure, as well as external factors such as background soil [41]. The S2 optical-image processing was carried out in Google Earth Engine (GEE) [15]. For Rwanda, going back to December 2018, GEE provides access to S2 images that are corrected to represent signal values at the bottom of the atmosphere. Values of reflectance in the four bands B2, B3, B4, and B8 (Table 3) were extracted from the identified imagery after cloud masking was applied using a built-in GEE algorithm and visually verifying the masked results. The S2 MSI offers 10-m ground resolution in these four selected bands [32].

S1 SAR image processing was also carried out in GEE. SAR images represent reflectance of electromagnetic radiation in the microwave range and are therefore not affected by cloud cover. For crops, this reflectance is primarily a function of the canopy architecture such as the size, shape, and orientation of canopy components; the dielectric properties of the crop canopy; and the cropping characteristics such as plant density and row direction [42]. GEE provides access to S1 images that are preprocessed with thermal-noise removal, radiometric calibration, and terrain correction. For this analysis, we selected images acquired using the Interferometric Wide (IW) swath mode and the

vertical transmit/vertical receive (VV) polarization. The S1 SAR instrument offers a 10-m ground resolution in this band [43].

Table 3. Specifications of optical bands selected for use in this study; S2-MSI has the ground resolution of 10 m for these bands.

S2 10-m Band	Central Wavelength (nm)	Bandwidth (nm)
B2 (Blue)	492	66
B3 (Green)	559	36
B4 (Red)	665	31
B8 (NIR)	833	106

2.4. Cropped Land Modeling

The training of the random forest (RF) model was carried out in GEE using built-in algorithms [44]. RF models have been widely used in interpreting remote sensing images because they produce accurate results, are computationally efficient, and can handle high data dimensionality without overfitting [45]. The model was parameterized using training data consisting of four S2 features and three S1 features for each of the labeled pixels. The S2 imagery from December 2018 through February 2019 was evaluated for cloud cover, and two images from late January were identified based on minimal cloud cover for the entire country (Table 4). The four S2 features were signal values in B2, B3, B4, and B8, extracted from a composite S2 image that was generated by filling in clouded pixels in the 2019-01-28 scene with unclouded pixels from the 2019-01-23 scene when available. The three S1 features were median VV values for the months of November 2018, December 2018, and January 2019. The training/testing datasets were generated from the ground-truth data using an 80/20 split.

Table 4. S2 imagery cloud cover by frame (information from Sentinel-hub EO-Browser); Rwanda falls within four S2 frames (35MQU: Kaberege, Ngarama; 35MRU: Cyampirita, Ngarama; 35MQT: Kinyaga, Rwakigarati; 35MRT: Kabarama).

S2 Flight Date	35MQU	35MRU	35MQT	35MRT
2018-12-04	77%	98%	93%	65%
2018-12-09	100%	100%	100%	100%
2018-12-14	44%	39%	19%	51%
2018-12-24	79%	87%	90%	76%
2018-12-29	39%	52%	19%	18%
2019-01-03	49%	29%	33%	21%
2019-01-08	37%	34%	36%	63%
2019-01-13	25%	12%	7%	14%
2019-01-18	81%	100%	100%	89%
2019-01-23	6%	12%	26%	7%
2019-01-28	31%	22%	13%	4%
2019-02-02	40%	40%	54%	35%
2019-02-07	91%	100%	82%	45%
2019-02-12	36%	77%	37%	66%
2019-02-17	99%	97%	98%	97%
2019-02-22	100%	100%	98%	99%
2019-02-27	35%	12%	12%	3%

3. Results

3.1. Discrimination of Labeled Categories

We analyzed signal values for the labeled categories in the Sentinel satellite imagery that contributed most to the between-class differentiation to better understand the feasibility of discriminating between selected categories of crops and ultimately to interpret the results of the ML model. The RF algorithm outputs a standardized measure of the importance of each of the features used in the model [45]. In our case, the S2-B3 and S2-B4 features were the most important for discriminating between the selected seven classes, followed by the S1-VV value. Box plots of the training data for each of the classes were created using the S2-B3, S2-B4, and S1-VV signal values (Figure 3a-c). Figure 3d shows a two-dimensional (2D) plot in the S2-B3 and S2-B4 coordinates for representative training points. Although there is significant overlap in the spectral signatures of beans, cassava, and other vegetation, maize, bananas, trees, and the non-vegetative class appear separable.

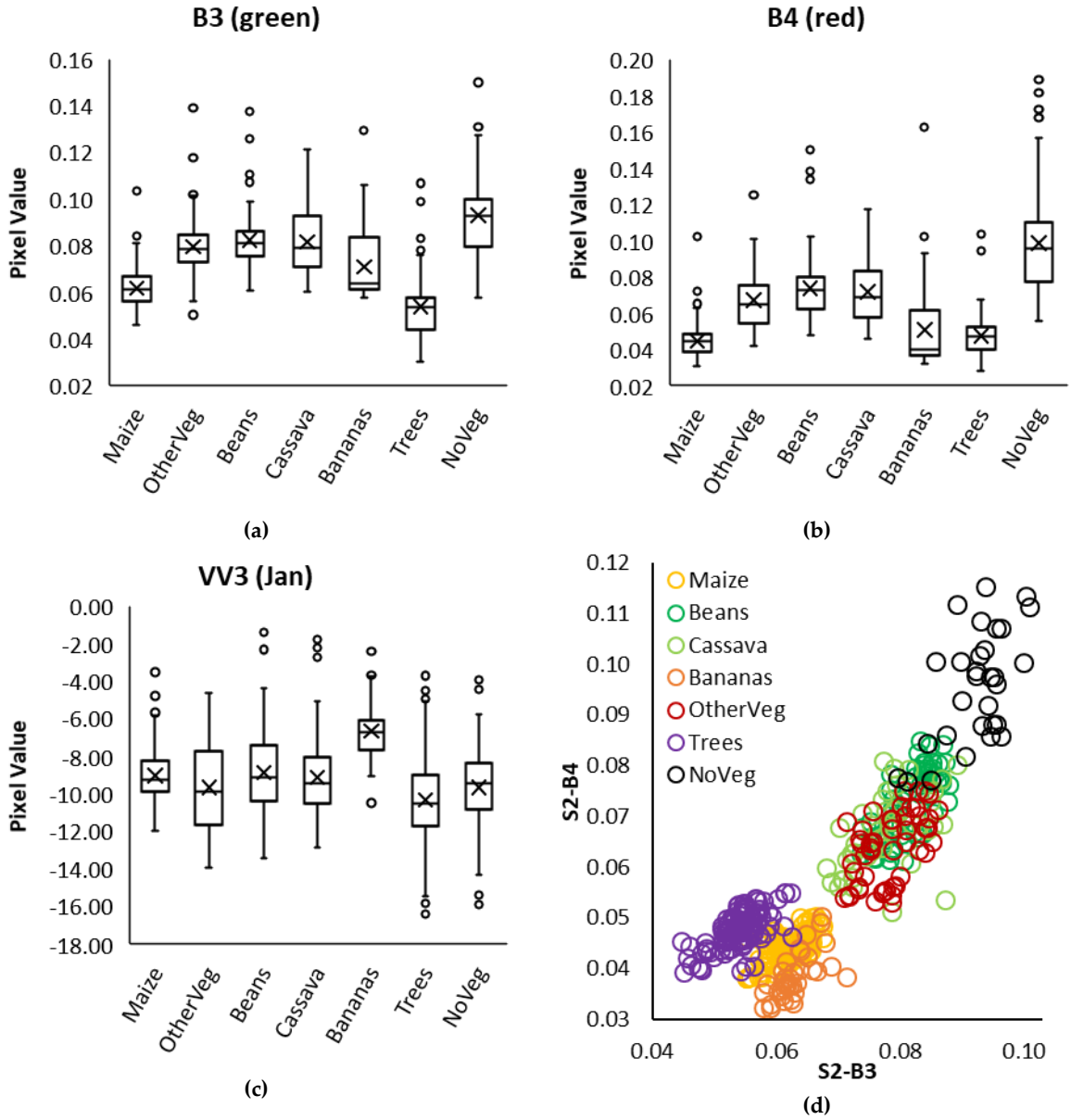

Figure 3. Boxplots of S2-MSI and S1-SAR features for all labeled training samples (a-c) and 2D S2-MSI feature space for representative training samples of each labeled class (d).

3.2. Intercropped Maize (iMaize)

A similar analysis was performed to compare spectral signatures of intercropped maize (denoted as iMaize) with the other agricultural categories. Maize in Rwanda is most often

intercropped with beans and cassava, although intercropping patterns can vary widely between fields both in terms of the crops being intercropped with maize and the ratio of maize to other crops (Figure 4). Given this variability and the relatively low density of maize in these examples, it is not surprising that such intercropped maize has a spectral signature that better matches the signature of the crop that it is intercropped with than the signature of pure maize (Figure 5). As a result, intercropped maize was likely classified as another crop type (i.e., beans or cassava). This is consistent with the labeling procedure used in this study in which we assigned the label according to the dominant crop type.

(a) (b)

Figure 4. Example of maize intercropped with cassava (a) and maize-only (b) fields in Rwanda. The 10-m x 10-m Sentinel grid cells are shown for reference and labeled to reflect at least 75% of the same landcover type.

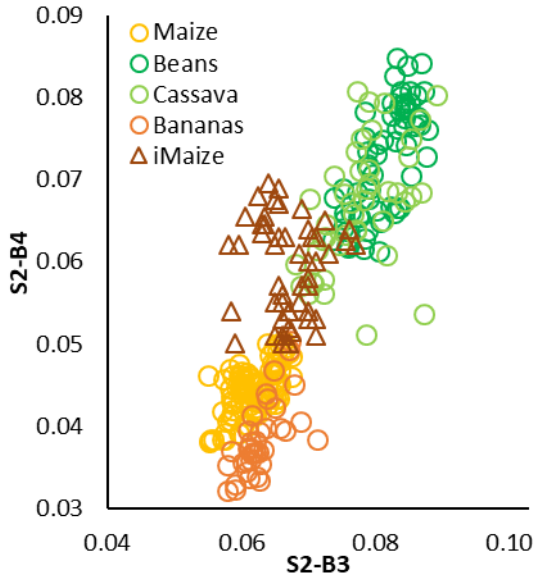

Figure 5. 2D S2-MSI feature space for representative examples of seasonal crops and vegetation (iMaize = intercropped maize).

3.3. Cropped Land Model Results

An RF model was trained and tested on the GEE platform using a composite image that consisted of four S2 features (B2, B3, B4, and B8) from a single point in time and three S1 features that spanned the peak of the growing season (median VV values for the months of November 2018,

December 2018, and January 2019). For the optical bands, pixels from the January 23 image were used to fill in clouded pixels in the January 28 image. The ground-truth dataset was split into training (80% of labeled points) and testing (20% of labeled points) datasets such that none of the points used to train the model were used to test the model. The confusion matrix for the testing dataset is provided in Table 5, where each row corresponds to a predicted class and each column to an actual class. The cells show the counts of correct and incorrect classifications for each class. The producer's accuracy, defined as the ratio of the number of sites classified correctly by the model to the total number of sites for the class, is shown in the last column. The overall accuracy of the model was 83%, with producer's accuracies of 91% and 84% for maize and beans, respectively.

Table 5. Confusion matrix for RF model; 95% confidence interval is provided for accuracy assessment.

Class	Maize	Beans	Cassava	Bananas	OtherVeg	Trees	NonVeg	% Accuracy
Maize	52	1	1	2	0	1	0	91 ± 4
Beans	1	16	2	0	0	0	0	84 ± 8
Cassava	1	1	12	1	1	0	2	67 ± 11
Bananas	2	0	1	11	0	1	0	73 ± 11
OtherVeg	1	4	2	1	21	1	0	72 ± 8
Trees	4	0	1	0	1	53	0	90 ± 4
NonVeg	0	5	1	0	0	0	16	73 ± 9
Total Pts	61	27	20	15	23	56	18	--

Examining the confusion matrix more closely, we can see that in cases where other vegetation was not classified correctly, it was most often confused with beans and cassava. These classes are spectrally very similar (Figure 3d), so this confusion is not surprising. The non-vegetative class was also confused with beans, and there is some spectral overlap with this class (Figure 3d). Trees were occasionally confused with maize, which again agrees with the short distance between data points corresponding to these categories (Figure 3d). The comparatively large confidence intervals for some of the categories (e.g., beans, cassava, and bananas) result from a relatively small number of data points used in the accuracy assessment based on the 80/20 split of the original ground-truth dataset. As discussed below, recommendations for larger scale follow-up studies include increasing the size of the training dataset by adding more categories to better capture growing conditions in Rwanda.

A cropped land area map (Figure 6) was created using the composite S1/S2 image for the entire country of Rwanda. National parks [46] and water bodies [47] were masked using available products in GEE. The estimated land area for each crop included in the model was compared with the 2019 Season A SAS at the country scale (Table 6) [36].

The estimated areas for maize and beans agreed with the crop/cultivated areas (defined as the area occupied by a given crop in a plot considering its density or occupation) reported in the SAS to within 3% and 7%, respectively. The estimated area for cassava was in good agreement with the total area reported by the SAS for tubers and roots but significantly overestimated the total area for cassava alone. The spectral feature space for cassava was overlapped with other vegetation, which was undercounted by the model. A large discrepancy was also observed for the predicted versus reported cropped area for bananas. The total harvested area (defined as the total number of hectares that was harvested in a given agricultural season) for bananas was lower than the cropped area (i.e., 82,523 ha versus 253,996 ha) indicating that the plants are at different stages of growth as would be expected for an annual crop. Other sources contributing to these discrepancies are further considered in the Discussion.

The total area under cultivation (i.e., the sum of classes 1 through 5) in the model (1,454,713 ha) agreed with the survey results (1,319,256 ha) to within 10%.

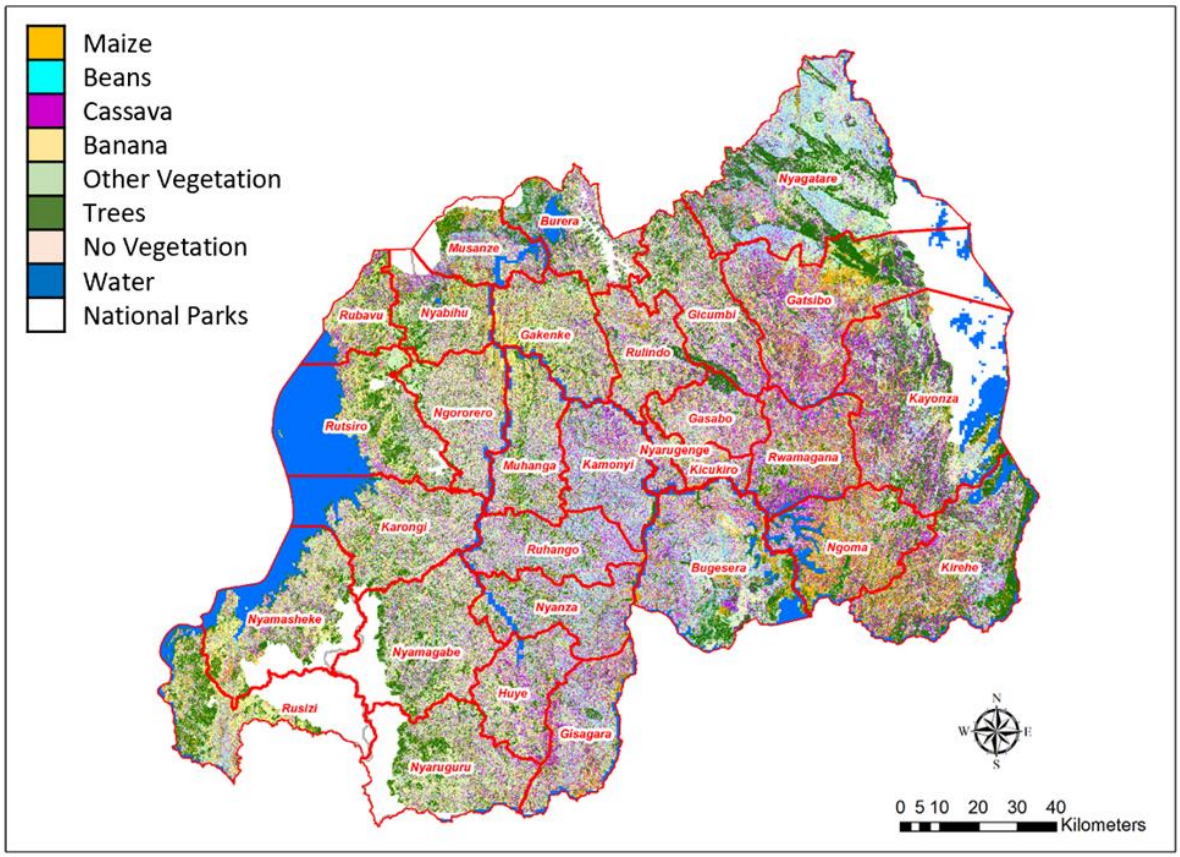

Figure 6. 2019 Season A crop area map.

Table 6. Comparison of areas under cultivation by selected crops predicted by the model to the cultivated area reported in the 2019A SAS.

Model Class	Model Area (ha)	SAS Category	2019A SAS (ha)	Difference
1. Maize	222,570	Maize	215,159	3%
2. Beans	319,548	Beans	299,443	7%
3. Cassava	322,060	Cassava	195,135	65%
4. Bananas	137,784	Bananas	253,996	−46%

4. Discussion

Up-to-date agricultural modeling and cropped land estimation are needed for planning (especially post-harvest activities) and price forecasting and identifying those at risk of food insecurity to inform resource allocation and sustainability efforts in developing countries. The Sentinel satellites provide free and timely data at a resolution that is appropriate for monitoring the smallholder agricultural systems that dominate these regions [5,6]. To map the satellite data to ground conditions for modeling, accurate information with respect to vegetation type and coverage is needed. Field surveys have traditionally been used to collect this information [6], but these methods are labor intensive, time consuming, and difficult to conduct in hilly terrain and other areas with poor road systems.

This pilot study investigated the use of UAVs for collecting high-fidelity ground-truth information for smallholder agricultural systems in Rwanda during the 2019 Season A. In total, 1,251 cells were labeled according to the dominant landcover, resulting in a ground-truth dataset that included strategic crops for food security and other vegetation types that are common in Rwanda. Using UAV imagery to develop labeled datasets has advantages over traditional methods involving observers on the ground, including the ability to georeference points more accurately and review

labels with respect to vegetation type, growth stage, and ground coverage. Labeling efforts can also be extended easily at any point after the images are obtained and points added to the datasets based on the purpose of a specific model. The labeling can also be automated as indicated by another recently published study from our group [38]. Limitations to collecting ground-truth examples in this manner include restrictions on site selection in terms of the elevation and slope at which UAVs can fly.

Although other studies that specifically address crop mapping in smallholder agricultural systems have focused on a single crop, most commonly maize [6], this study aimed to develop a cropped area map that included several strategic crops. To gain insight into the feasibility of discriminating between different crops and to aid in the interpretability of the model, we analyzed spectral signatures of the different crops at the peak of the season in selected optical and SAR bands. This qualitative analysis indicated that maize, bananas, trees, and the non-vegetative class were well separated, but beans, cassava, and other vegetation significantly overlapped. We also examined spectral signatures of plots of maize that were intercropped with beans or cassava. From the UAV imagery, we determined that there was a broad range of intercropping patterns. Not surprisingly, when the density of maize was low, the plot signature more closely matched that of beans or cassava compared with pure maize. To better capture intercropped conditions, researchers should include additional categories and ground-truth examples in the model to describe specific intercropping patterns. Ultimately, as the development of publicly supported satellite networks continues and more high-resolution imagery is made freely available, the accuracy of labeled datasets and ML models will improve. For example, Richard et al. were able to differentiate between pure maize and intercropped maize conditions using imagery acquired from the commercial RapidEye satellites that provide images with 5-m ground resolution [43].

The ground-truth dataset generated from the labeled UAV imagery was used to create a cropped land model using a S1/S2 composite image. The RF model was developed using the open-access GEE platform and achieved an overall accuracy of 83%, and maize and beans (including climbing beans and bush beans) were classified with overall accuracies of 91% and 84%, respectively. In contrast to similar models created for other countries with smallholder systems, this model provided information on more than one crop. For example, although the seminal studies by Jin et al. and Burke et al. [4-6] focused on maize, the model presented here included maize, beans, cassava, and bananas. Model accuracies for these categories compare well to the models reported in the other studies of smallholder agricultural systems, in which single crops were classified with accuracies ranging from 67% to 79% [4-6]. To tighten the confidence interval and improve accuracies for individual categories, labeling efforts should be expanded in future full-scale studies. Ideally, independently gathered ground-truth data (especially for testing) would also be incorporated into a full-scale study to highlight and remove any biases in the model.

To further assess the model, we compared crop-specific areas calculated by the model with areas reported by the SAS for the same 2019 Season A. Although the estimated areas for maize and beans agreed with the survey results, the estimated area for cassava did not. The classification accuracy of cassava was lower than the other classes included in the model. The spectral signature of cassava overlapped with the spectral signature of the "other vegetation" class, which was under-counted by the model compared to the 2019 SAS. Additionally, some of intercropped maize was likely counted as cassava based on the similarity in spectral information.

Although not a major source of testing error in the RF model, bananas were undercounted in relation to the 2019A SAS. Again, the harvested area was less than the total cropped area; 32% of the crop was harvested during Season A. The examples of bananas included in the training set were all from mature, healthy plants. Additionally, we did not include banana plants that were growing in residential areas, which is commonly practiced in Rwanda. To reduce noise in the training dataset, we decided early in the labeling effort to include only cells that were dominated (i.e., at least 75%) by a single class type, and we included only cells with banana plants that were surrounded by other cells with banana plants. Banana plants that were growing next to structures were likely classified in the non-vegetative class in our model because it was the dominant landcover. Again, as more higher

resolution satellite imagery becomes available, the addition of mixed-landcover classes to the labeling taxonomy will help capture bananas growing in residential areas.

In the process of creating the country-scale map, we used existing shapefiles of water bodies and national parks to mask out known areas. The accuracy of these shapefiles affects the accuracy of the land areas calculated from the map generated using the trained ML model. Therefore, as these shapefiles are updated and improved, the precision of any models downstream in the mapping process will benefit. Future studies will be positively affected by the availability of up-to-date shapefiles for urban areas and other large-area non-vegetative structures that do not change as quickly as agricultural regions. These shapefiles can be created using commercial imagery as a source of ground-truth datasets for training the model, leaving UAV-acquired imagery for ground truthing of areas of intensive agricultural growth.

5. Conclusions

This pilot study indicates the potential to use UAV-acquired imagery rather than traditional ground-observer methods to collect large amounts of accurate ground-truth data. When collected via UAVs, ground-truth locations can be georeferenced accurately, which is important in areas where individual plots are small (<1 ha) and intercropping is the predominant practice. Additionally, imagery can be reviewed to verify ground cover and extract different features such as density of vegetation coverage. More examples can easily be added to the training and testing datasets at any time based on the intent of the model. Limitations to collecting ground-truth examples in this manner include restrictions on site selection in terms of the elevation and slope at which UAVs can fly and regulatory constraints.

The UAV-based ground-truth dataset was used for training and testing an ML model for seven selected landcover categories, including four key crops in Rwanda. The overall accuracy of the model was 83%, with accuracies of 91% and 84% for maize and beans, respectively. Cassava was classified with lower accuracy (67%), and the model tended to confuse it with the catch-all class of other vegetation. Model accuracy may be improved by creating mixed land use categories to better capture intercropping and bananas growing in residential areas.

Future work will benefit from further increasing the size of the ground-truth datasets (note: our sample size included 1,251 total examples that were divided between training and testing datasets) and adding categories to the limited taxonomy we worked with. The addition of these categories will need to be accompanied by an increase in the number of data points assuming 100 samples per class and ideally per AEZ as a typical rule of thumb for the minimum size. Further attention needs to be given to creating accurate and up-to-date shapefiles for landcover categories that do not require the resolution and timeliness needed for agricultural areas. The availability of these shapefiles will allow the downstream models to focus on agricultural classes and improve the overall classification accuracy.

Author Contributions: Data curation, Jason Polly, Margret O'Neil, and Noel Ujeneza; Formal analysis, Meghan Hegarty-Craver, Jason Polly, and Dorota Temple; Investigation, James Rineer, Robert Beach, Daniel Lapidus, and Dorota Temple; Methodology, Noel Ujeneza, James Rineer, Robert Beach, Daniel Lapidus, and Dorota Temple; Software, Meghan Hegarty-Craver, Jason Polly, and Margret O'Neil; Project administration and supervision, James Rineer, Robert Beach, Daniel Lapidus, and Dorota Temple. All authors have read and agreed to the published version of the manuscript.

Funding: This research received no external funding.

Acknowledgments: We gratefully acknowledge the financial support of RTI International through its Grand Challenge Initiative. We have benefited greatly from discussions with stakeholders in the Government of Rwanda, United States Agency for International Development, United Kingdom Department for International Development, European Union, World Bank, UN Food and Agriculture Organization, and many non-government organizations operating in Rwanda. Mads Knudsen from Vanguard Economics also provided important support to advance this analysis. We thank Charis Unmanned Aerial Solutions for executing UAV flights.

Conflicts of Interest: The authors declare no conflicts of interest.

References

1. Macdonald, R.B. A summary of the history of the development of automated remote sensing for agricultural applications. *IEEE Trans Geosci Remote Sens* **1984**, *GE-22*, 473-482.
2. Frey, H.T.; Mannering, J.V.; Burwell, R.E. *Agricultural Application of Remote Sensing: the Potential from Space Platforms*. Economic Research Service, US Department of Agriculture: 1949.
3. Foley, M. What and why, but not how, the climate solutions consensus: what we know and what to do about it. *Ecol Econ* **2011**, *70*, 2534-2534.
4. Burke, M.; Lobell, D.B. Satellite-based assessment of yield variation and its determinants in smallholder African systems. *Proc Natl Acad Sci U S A* **2017**, *114*, 2189-2194.
5. Jin, Z.; Azzari, G.; Burke, M.; Aston, S.; Lobell, D. Mapping smallholder yield heterogeneity at multiple scales in Eastern Africa. *Remote Sens* **2017**, *9*.
6. Jin, Z.; Azzari, G.; You, C.; Di Tommaso, S.; Aston, S.; Burke, M.; Lobell, D.B. Smallholder maize area and yield mapping at national scales with Google Earth Engine. *Remote Sens Environ* **2019**, *228*, 115-128.
7. Temple, D.S.; Polly, J.S.; Hegarty-Craver, M.; Rineer, J.I.; Lapidus, D.; Austin, K.; Woodward, K.P.; Beach III, R.H. *The View from Above: Satellites Inform Decision-Making for Food Security*; RTI Press Publication No. RB-0021-1908; RTI International: Research Triangle Park, NC, 2019.
8. The Sen2-agri system. Available online: http://www.esa-sen2agri.org/ (accessed on 20 March 2020).
9. Gorelick, N.; Hancher, M.; Dixon, M.; Ilyushchenko, S.; Thau, D.; Moore, R. Google Earth Engine: planetary-scale geospatial analysis for everyone. *Remote Sens Environ* **2017**, *202*, 18-27.
10. Food and Agriculture Organization of the United Nations (FAO). *Global Strategy to Improve Agricultural and Rural Statistics, Action Plan, 2020-2025*; Rome, Italy, 2018.
11. Global Strategy to Improve Agricultural and Rural Statistics (GSARS). *Handbook on Remote Sensing for Agricultural Statistics*; Rome, Italy, 2017.
12. Fritz, S.; See, L.; You, L.; Justice, C.; Becker-Reshef, I.; Bydekerke, L.; Cumani, R.; Defourny, P.; Erb, K.; Foley, J., *et al.* The need for improved maps of global cropland. *Trans Am Geophys Union* **2013**, *94*, 31-32.
13. Liakos, K.G.; Busato, P.; Moshou, D.; Pearson, S.; Bochtis, D. Machine learning in agriculture: a review. *Sensors (Basel)* **2018**, *18*.
14. Vijayasekaran, D. Sen2-Agri – crop type mapping pilot study using sentinel-2 satellite imagery in India. *ISPRS - International Archives of the Photogrammetry, Remote Sensing and Spatial Information Sciences* **2019**, *XLII-3/W6*, 175-180.
15. Shelestov, A.; Lavreniuk, M.; Kussul, N.; Novikov, A.; Skakun, S. Exploring Google Earth engine platform for big data processing: classification of multi-temporal satellite imagery for crop mapping. *Front Earth Sci* **2017**, *5*.
16. Veloso, A.; Mermoz, S.; Bouvet, A.; Le Toan, T.; Planells, M.; Dejoux, J.-F.; Ceschia, E. Understanding the temporal behavior of crops using Sentinel-1 and Sentinel-2-like data for agricultural applications. *Remote Sens Environ* **2017**, *199*, 415-426.
17. Joint experiment for crop assessment and monitoring. Available online: http://jecam.org/ (accessed on 19 March 2020).
18. Belgiu, M.; Csillik, O. Sentinel-2 cropland mapping using pixel-based and object-based time-weighted dynamic time warping analysis. *Remote Sens Environ* **2018**, *204*, 509-523.

19. Csillik, O.; Belgiu, M. Cropland mapping from Sentinel-2 time series data using object-based image analysis, Proceedings of the 20th AGILE International Conference on Geographic Information Science Societal Geo-innovation: Celebrating 20 years of GIS research!, Wageningen, Netherlands, 2017; Wageningen, Netherlands.
20. Xiong, J.; Thenkabail, P.S.; Tilton, J.C.; Gumma, M.K.; Teluguntla, P.; Oliphant, A.; Congalton, R.G.; Yadav, K.; Gorelick, N. Nominal 30-m cropland extent map of continental Africa by integrating pixel-based and object-based algorithms using sentinel-2 and landsat-8 data on Google Earth Engine. *Remote Sens* **2017**, *9*.
21. Sonobe, R.; Yamaya, Y.; Tani, H.; Wang, X.; Kobayashi, N.; Mochizuki, K.-i. Assessing the suitability of data from Sentinel-1A and 2A for crop classification. *GISci Remote Sens* **2017**, *54*, 918-938.
22. Sonobe, R.; Yamaya, Y.; Tani, H.; Wang, X.; Kobayashi, N.; Mochizuki, K.-i. Crop classification from Sentinel-2-derived vegetation indices using ensemble learning. *J Appl Remove Sens* **2018**, *12*, 026019.
23. Shi, Y.; Thomasson, J.A.; Murray, S.C.; Pugh, N.A.; Rooney, W.L.; Shafian, S.; Rajan, N.; Rouze, G.; Morgan, C.L.; Neely, H.L., *et al.* Unmanned aerial vehicles for high-throughput phenotyping and agronomic research. *PLoS One* **2016**, *11*, e0159781.
24. Eckman, S.; Eyerman, J.; Temple, D. *Unmanned Aircraft Systems Can Improve Survey Data Collection*; RTI Press Publication No. RB-0018-1806; RTI International: Research Triangle Park, NC, 2018.
25. Bigirimana, F. (National Institute of Statistics Rwanda). Personal communication. 2019.
26. Yang, M.-D.; Huang, K.-S.; Kuo, Y.-H.; Tsai, H.; Lin, L.-M. Spatial and spectral hybrid image classification for rice lodging assessment through UAV imagery. *Remote Sens* **2017**, *9*.
27. Yahyanejad, S.; Rinner, B. A fast and mobile system for registration of low-altitude visual and thermal aerial images using multiple small-scale UAVs. *ISPRS J Photogramm Remote Sens* **2015**, *104*, 189-202.
28. Lelong, C.C.; Burger, P.; Jubelin, G.; Roux, B.; Labbe, S.; Baret, F. Assessment of unmanned aerial vehicles imagery for quantitative monitoring of wheat crop in small plots. *Sensors (Basel)* **2008**, *8*, 3557-3585.
29. Baluja, J.; Diago, M.P.; Balda, P.; Zorer, R.; Meggio, F.; Morales, F.; Tardaguila, J. Assessment of vineyard water status variability by thermal and multispectral imagery using an unmanned aerial vehicle (UAV). *Irrigation Sci* **2012**, *30*, 511-522.
30. Hall, O.; Dahlin, S.; Marstorp, H.; Archila Bustos, M.; Öborn, I.; Jirström, M. Classification of maize in complex smallholder farming systems using UAV imagery. *Drones* **2018**, *2*.
31. Tripicchio, P.; Satler, M.; Dabisias, G.; Ruffaldi, E.; Avizzano, C.A. Towards smart farming and sustainable agriculture with drones. In *2015 International Conference on Intelligent Environments*, 2015; pp 140-143.
32. Polly, J.; Hegarty-Craver, M.; Rineer, J.; O'Neil, M.; Lapidus, D.; Beach, R.; Temple, D.S. The use of Sentinel-1 and -2 data for monitoring maize production in Rwanda. *Proceedings of SPIE* **2019**.
33. National ICT4RAg strategy (2016-2020). Available online: http://www.minagri.gov.rw/fileadmin/user_upload/documents/policies_and_strategy/ICT4RAg_STRATEGIC_PLAN_2016-2020_final__final__3_.pdf (accessed on 20 March 2020).
34. Strategies for sustainable crop intensification in Rwanda. Available online: http://www.minagri.gov.rw/fileadmin/user_upload/documents/CIP/CIP_Strategies_2011.pdf (accessed on 20 March 2020).
35. Strategic plan for the transformation of agriculture in Rwanda – phase II (PSTA II) final report. Available online:

http://www.minagri.gov.rw/fileadmin/user_upload/documents/RWANDA_SAKSS/PSTA_II__2008-12_.pdf (accessed on 20 March 2020).

36. National Institute of Statistics of Rwanda. Seasonal agricultural survey. Season A 2019 report. March 2019.
37. National Institute of Statistics of Rwanda. Gross domestic product—2019. Available online: http://www.statistics.gov.rw/publication/gdp-national-accounts-2019 (accessed on 22 April 2020).
38. Chew, R.; Rineer, J.; Beach, R.; O'Neil, M.; Ujeneza, N.; Lapidus, D.; Miano, T.; Hegarty-Craver, M.; Polly, J.; Temple, D.S. Deep neural networks and transfer learning for food crop identification in UAV images. *Drones* **2020**, *4*.
39. Rushemuka, P.N.; Bock, L.; Mowo, J.G. Soil science and agricultural development in Rwanda: state of the art. A review. *BASE* **2014**, *18*, 142-154.
40. Prasad, P.V.; Hijmans, R.J.; Pierzynski, G.M.; Middendorf, J.B. *Climate Smart Agriculture and Sustainable Intensification: Assessment and Priority Setting for Rwanda*; Kansas State University: Manhattan, KS, 2016.
41. Jensen, J.R. *Remote Sensing of the Environment*. 2 ed.; Pearson Prentice Hall: Upper Saddle River, NJ, 2007.
42. Kumaraperumal, R.; Shama, M.; Ragunath, B.; Jagadeeswaran, R. Sentinel 1A SAR backscattering signature of maize and cotton crops. *Madras Agric J* **2017**, *104*, 54-57.
43. Richard, K.; Abdel-Rahman, E.M.; Subramanian, S.; Nyasani, J.O.; Thiel, M.; Jozani, H.; Borgemeister, C.; Landmann, T. Maize cropping systems mapping using rapideye observations in agro-ecological landscapes in Kenya. *Sensors (Basel)* **2017**, *17*.
44. Machine learning in earth engine. Available online: https://developers.google.com/earth-engine/machine-learning (accessed on 3 March 2020).
45. Belgiu, M.; Drăguţ, L. Random forest in remote sensing: a review of applications and future directions. *ISPRS J Photogramm Remote Sens* **2016**, *114*, 24-31.
46. WDPA: World Database on Protected Areas (polygons). Available online: https://developers.google.com/earth-engine/datasets/catalog/WCMC_WDPA_current_polygons (accessed on 20 March 2020).
47. Copernicus global land cover layers: CGLS-LC100 collection 2. Available online: https://developers.google.com/earth-engine/datasets/catalog/COPERNICUS_Landcover_100m_Proba-V_Global (accessed on 20 March 2020).